


# The topological susceptibility and excess kurtosis in SU(3) Yang-Mills theory

Stephan Dürr <sup>a,b</sup> and Gianluca Fuwa<sup>a</sup>

<sup>a</sup>Department of Physics, University of Wuppertal, 42119 Wuppertal, Germany

<sup>b</sup>Jülich Supercomputing Centre, Forschungszentrum Jülich, 52425 Jülich, Germany

## Abstract

We determine the topological susceptibility and the excess kurtosis of  $SU(3)$  pure gauge theory in four space-time dimensions. The result is based on high-statistics studies at seven lattice spacings and in seven physical volumes, allowing for a controlled continuum and infinite volume extrapolation. We use a gluonic topological charge measurement, with gradient flow smoothing in the operator. Two complementary smoothing strategies are used (one keeps the flow time fixed in lattice units, one in physical units). Our data support a recent claim that both strategies yield a universal continuum limit; we find  $\chi_{\text{top}}^{1/4} r_0 = 0.4769(14)(11)$  or  $\chi_{\text{top}}^{1/4} = 197.8(0.7)(2.7)$  MeV.

## 1 Introduction

Yang-Mills (YM) theories in four space-time dimensions dynamically generate a scale by a process called “dimensional transmutation” [1]. This scale reflects itself in any dimensionful quantity, for instance the topological susceptibility  $\chi_{\text{top}} = \lim_{V \rightarrow \infty} \langle q^2 \rangle / V$ . Here  $q$  is the (global) topological charge of the gauge background (see below) and  $V$  the volume of the four-dimensional Euclidean box.

The topological susceptibility has the dimension  $\text{MeV}^4$ , and our goal is to calculate (from first principles) the ratio of  $\chi_{\text{top}}^{1/4}$  and another dimensionful quantity for  $N_c = 3$  colors (the result has no free parameters). In this work we select the inverse of the Sommer radius  $r_0$  [2] to set the scale, so we calculate  $\chi_{\text{top}}^{1/4} r_0$ . We choose this option, because there is a practical parametrization<sup>1</sup> of  $r_0/a$ , where  $a$  is the lattice spacing, in the appendix of Ref. [6], which, in turn, is based on data from Ref. [7].

The motivation to study the topological susceptibility in QCD-like theories is two-fold. On the one hand,  $\chi_{\text{top}}$  serves as a vacuum diagnostics tool. In YM theory it depends on  $N_c$ , while in QCD it depends on  $N_c$  and the  $N_f$  individual quark masses (see Refs. [8, 9] for details). On the other hand, the YM susceptibility appears in the Witten-Veneziano formula [10, 11]

$$\chi_{\text{top}}^{\text{YM}} \doteq \frac{F^2}{2N_f} (M_{\eta'}^2 + M_{\eta}^2 - 2M_K^2) \quad (1)$$

which is supposed to hold at leading order in the  $1/N_c$  expansion. Interestingly, the right-hand side refers to full QCD quantities<sup>2</sup> only, so the relation links two distinct theories.

---

<sup>1</sup>In principle the rooted string tension  $\sigma^{1/2}$  or the glueball mass  $M_{0^{++}}$  or an artificial scale like  $t_0^{-1/2}$  [3, 4] or  $w_0^{-1}$  [5] would be equally well suited, but for these quantities we are unaware of a similarly convenient parametrization.

<sup>2</sup>We use the Bern normalization  $F_\pi = f_\pi/\sqrt{2}$  of the pion decay constant, where  $F_\pi^{\text{phys}} = 92.4(3)$  MeV in QCD with physical quark masses, and  $F = 86.2(5)$  MeV in the 2-flavor chiral limit [12].

In the continuum the topological susceptibility in a finite Euclidean volume  $V$  may be defined as

$$\chi_{\text{top}} = \int \langle q(x)q(0) \rangle d^4x = \lim_{p^2 \rightarrow 0} \frac{1}{V} \int \langle q(x)q(y) \rangle e^{ip(x-y)} d^4x d^4y \quad (2)$$

where  $q(x)$  is the topological charge density. In this approach two limits are involved, zero virtuality ( $p^2 \rightarrow 0$ ) and infinite volume ( $V \rightarrow \infty$ ) in toroidal geometry. Alternatively, one may use the definition

$$\chi_{\text{top}} = \frac{\langle q^2 \rangle}{V} \quad \text{with} \quad q = \int q(x) d^4x \quad (3)$$

the global topological charge  $q \in \mathbb{Z}$ . Again a limit  $V \rightarrow \infty$  is required, but now one is restricted to  $p^2 = 0$ . The two approaches are equivalent (up to a possible contact term [13]).

On the lattice one may start from definitions analogous to (2) or (3), but the renormalization details are different for these apparently similar options. With

$$\begin{aligned} q_{\text{nai}}(x) &= \frac{1}{32\pi^2} \epsilon_{\mu\nu\rho\sigma} \text{Tr}[F_{\mu\nu}(x)F_{\rho\sigma}(x)] \\ &= \frac{1}{4\pi^2} \text{Tr}[F_{12}(x)F_{34}(x) - F_{13}(x)F_{24}(x) + F_{14}(x)F_{23}(x)] \end{aligned} \quad (4)$$

a gluonic definition of the field-strength tensor  $F_{\mu\nu}(x) = F_{\mu\nu}(x)^a T^a$  with  $T^a = \frac{1}{2}\lambda^a$  and thus of the *local* topological charge density  $q(x)$  is chosen. In this case the topological susceptibility

$$\chi_{\text{top}} = Z_q^2(\beta)\chi_{\text{nai}} + M(\beta) \quad \text{with} \quad \chi_{\text{nai}} = \frac{a^4}{N} \sum_{x,y \in \Lambda} q_{\text{nai}}(x)q_{\text{nai}}(y) \quad (5)$$

akin to (2) renormalizes both<sup>3</sup> multiplicatively and additively [17–19]. Here  $N = (L/a)^4$  is the number of lattice sites, while  $V = L^4$  is the box volume in physical units. Alternatively

$$q_{\text{ren}} = \text{round}(Z_q(\beta)q_{\text{nai}}) \quad \text{with} \quad q_{\text{nai}} = a^4 \sum_{x \in \Lambda} q_{\text{nai}}(x) \quad (6)$$

is a gluonic definition of the *global* topological charge  $q$  which renormalizes only<sup>4</sup> multiplicatively. Based on  $q_{\text{ren}}$  as defined in (6) one may proceed to define the topological susceptibility

$$\chi_{\text{top}} = \frac{\langle q_{\text{ren}}^2 \rangle}{V} \quad (7)$$

akin to (3) without further ado. Since  $q_{\text{ren}}$  is a fully renormalized quantity, no further renormalization is needed in this second step. This second approach is technically simpler and thus popular [6, 20–23], but the price to pay is that one is restricted to quantities at zero virtuality. We use it in this article, but we shall address higher moments of the global charge distribution, such as the excess kurtosis  $\langle q^4 \rangle / \langle q^2 \rangle - 3\langle q^2 \rangle$ , based on the renormalized global topological charge (6).

The remainder of this article is organized as follows. In Sec. 2 we specify how we smooth the gauge configurations to define a variety of  $q_{\text{nai}} \in \mathbb{R}$  and  $q_{\text{ren}} \in \mathbb{Z}$  which is less susceptible to UV noise. In

<sup>3</sup>Still within the local approach, one may use a fermionic definition of the topological charge density, specifically  $q_{\text{fer}}(x) = \text{Tr}(\gamma_5(1 - \frac{aD(x,x)}{2\rho})) = -\frac{1}{2\rho} \text{Tr}(\gamma_5 aD(x,x))$  where  $D$  is the overlap Dirac operator at projection parameter  $\rho \simeq 1$ , and the trace is over color and spinor indices only. In this case no further renormalization is needed [14–16].

<sup>4</sup>An additive renormalization of  $q_{\text{nai}}$  is excluded by the CP symmetry of the lattice theory. With overlap fermions things are even simpler, since  $q_{\text{fer}} = a^4 \sum_{x \in \Lambda} q_{\text{fer}}(x)$  is already integer valued and does not require any renormalization.

Sec. 3 we discuss how we choose the bare parameters to generate a number of ensembles with a joint physical volume and a series of decreasing lattice spacings, and we give details of how we compute the  $Z_q$ -factors for the global topological charge. In Sec. 4 our analysis is presented which yields the continuum limit of the topological susceptibility in a fixed physical volume, together with a robust estimate of the theoretical uncertainty involved. In Sec. 5 the same type of analysis is repeated for the excess kurtosis of the global charge distribution. In Sec. 6 we use another set of simulations to study the infinite volume behavior of the quantities studied in the previous two sections, again with a careful estimate of the theoretical uncertainty involved. Finally, in Sec. 7 some conclusions are given and prospects for some future research are discussed.

## 2 Smoothing via stout smearing or Wilson flow

In contemporary lattice field theory two closely related smoothing schemes are used, stout smearing [24] and gradient flow [3, 4, 25]. We use the output  $V_\mu(x)$  of either one to define a clover operator

$$\begin{aligned}
C_{\mu\nu}(x) &= V_\mu(x)V_\nu(x + \hat{\mu})V_\mu^\dagger(x + \hat{\nu})V_\nu^\dagger(x) \\
&+ V_\nu(x)V_\mu^\dagger(x - \hat{\mu} + \hat{\nu})V_\nu^\dagger(x - \hat{\mu})V_\mu(x - \hat{\mu}) \\
&+ V_\mu^\dagger(x - \hat{\mu})V_\nu^\dagger(x - \hat{\mu} - \hat{\nu})V_\mu(x - \hat{\mu} - \hat{\nu})V_\nu(x - \hat{\nu}) \\
&+ V_\nu^\dagger(x - \hat{\nu})V_\mu(x - \hat{\nu})V_\nu(x + \hat{\mu} - \hat{\nu})V_\mu^\dagger(x)
\end{aligned} \tag{8}$$

for a given lattice site  $x \in \Lambda$ . Here  $\hat{\mu}$  denotes  $a$  times the unit vector in the direction  $\mu$ . This  $C_{\mu\nu}(x)$  is to be identified with  $4I_{N_c}$  plus  $4i$  times the field-strength operator. Unlike  $F_{\mu\nu}(x)$  in the continuum<sup>5</sup> it is not exactly hermitean (in color space) and not exactly traceless. Therefore we define

$$F_{\mu\nu}(x) = P_{\text{TH}}\left[\frac{1}{4i}C_{\mu\nu}(x)\right] \quad \text{with} \quad P_{\text{TH}}[M] = \frac{1}{2}(M + M^\dagger) - \frac{1}{2N_c}\text{Tr}(M + M^\dagger)I_{N_c} \tag{9}$$

as the traceless hermitean part of (8) divided by  $4i$ .

Our smeared field  $V_\mu(x)$  emerges from the unsmeared  $U_\mu(x)$  through  $n$  steps of stout<sup>6</sup> smearing

$$V_\mu(x) = V_\mu^{(n)}(x), \quad V_\mu^{(n)}(x) = e^{i\rho Q_\mu^{(n-1)}(x)} V_\mu^{(n-1)}(x), \quad V_\mu^{(0)}(x) = U_\mu(x) \tag{10}$$

where the stout parameter should be chosen in the interval  $0 < \rho < 0.125$  in 4D [26]. The operator

$$Q_\mu^{(n-1)}(x) = P_{\text{TH}}\left[\frac{1}{i}S_\mu^{(n-1)}(x)V^{(n-1)\dagger}(x)\right] \tag{11}$$

contains the product of  $V_\mu(x)$  and  $S_\mu^\dagger(x)$  which also appears in the Wilson gauge action, with

$$S_\mu^{(k)}(x) = \sum_{\nu \neq \mu} \left\{ V_\nu^{(k)}(x)V_\mu^{(k)}(x + \hat{\nu})V_\nu^{(k)\dagger}(x + \hat{\mu}) + V_\nu^{(k)\dagger}(x - \hat{\nu})V_\mu^{(k)}(x - \hat{\nu})V_\nu^{(k)}(x + \hat{\mu} - \hat{\nu}) \right\} \tag{12}$$

being the staple around the link  $V_\mu(x)$ , pointing in the same direction as the link itself.

The main advantage of stout smearing is that one stays in the gauge group, hence no ‘‘backprojection’’ to  $SU(3)$  is needed. This is the technical basis of the suggestion made in Refs. [3, 4, 25]

<sup>5</sup>We like observables like the field-strength  $F_{\mu\nu}(x)$  or the gauge potential  $A_\mu(x)$  in  $U_\mu(x) = P\{\exp[ig \int_x^{x+\hat{\mu}} A(s) ds]\}$  to be hermitean quantities, as is common practice in quantum mechanics.

<sup>6</sup>Alternatively, one may remove the  $i$  and  $1/i$  in (10, 11) and replace  $P_{\text{TH}}$  by the traceless antihermitean projector.

to consider the limit  $\rho \rightarrow 0$  and  $n \rightarrow \infty$  where the product  $n \times \rho = t/a^2$  is kept constant. The quantity  $t/a^2$  is called the “flow time in lattice units” and has the meaning of a cumulative sum of the  $\rho$ -parameters used in all steps. Hence, to reach  $t/a^2 = 0.84$  one may factor the sum as  $7 \times 0.12$  or  $14 \times 0.06$  or  $28 \times 0.03$ , and so on. In this sequence the discretization error in the flow time decreases (ideal Wilson flow is the error-free limit). For some applications (e.g. the determination of  $t_0$  [3, 4] or  $w_0$  [5]) it is important to keep the flow time discretization effect small. For other applications (e.g. the one we have in mind) it is less important (we shall come back to this point in Sec. 3). The matching between stout smearing and (ideal) Wilson flow has been discussed in Refs. [4, 23, 27, 28].

In today’s lattice literature the main difference between “stout smearing” and “gradient flow” is the quantity which is held fixed in the continuum limit  $a \rightarrow 0$ . The terminology “stout smearing” usually implies that  $\rho$  and  $n$ , and hence the flow time  $t/a^2$  in *lattice units* is kept constant at all  $\beta$ . With this strategy the naive topological charge density (4) is an ultra-local operator (fixed footprint in lattice units) at all  $\beta$ , and becomes point-like in the limit  $a \rightarrow 0$ . The terminology “gradient flow” is usually chosen when the flow time  $t/r_0^2 = t/a^2 \times (a/r_0)^2$  in *physical units* is held fixed at all  $\beta$ . In our approximation (via stout smearings with  $\rho$  fixed) the number of steps is then bound to increase like  $(r_0/a)^2$  towards the continuum. As a result,  $q_{\text{nai}}(x)$  is “regularized” over a distance  $\sqrt{8t}$  (which is a fixed distance in  $r_0$  units) and no longer ultra-local [3]. Hence, in this strategy a second regulator is in place, which persists in the continuum limit  $a \rightarrow 0$ , see e.g. Ref. [28] for a discussion.

In Ref. [29] it is claimed that the topological susceptibility  $\chi_{\text{top}}$  is a “special observable” in the sense that the continuum limit can be taken at a fixed flow time in physical units, too, not just at a fixed flow time in lattice units (as was traditionally done). In other words, the claim is that for this observable the additional flow regulator does not introduce any systematic bias (the continuum extrapolated value  $\chi_{\text{top}} r_0^4$  at fixed  $t/r_0^2$  would be the same as, say, with 7 stout steps), provided  $\sqrt{t}$  is in a range where it smoothes out short-range fluctuations but leaves long-range fluctuations (say for  $r > r_0$ ) unaffected. In this article we plan to confront this assertion with numerical data.

### 3 Lattice setup and renormalization factors

Our goal is to set up a series of lattice simulations with a fixed physical volume. We choose  $V = (2.4783 r_0)^4$  which is about 51% larger than the volume  $V = (2.2356 r_0)^4$  of Ref. [6]. We use the Wilson gauge action, and Eq. (14) of Ref. [6] parametrizes  $r_0/a$  as a function of  $\beta$ . With this formula it is easy to compile a list of  $(L/a, \beta)$  combinations which realize  $L = 2.4783 r_0$ . Today,  $t_0$  [3, 4] is more popular to set the scale, but we are unaware of an equally handy parametrization, and we see no reason to believe that the continuum limit would be different<sup>7</sup> at all.

Details of our plan are presented in Tab. 1. We use three smoothing strategies, named “7 stout” (fixed  $t/a^2 = 0.84$ ) and “0.21 fm”, “0.30 fm” (fixed  $t/r_0^2$ ), respectively. To get statistically independent continuum extrapolated values, we shall generate  $7 \times 3 = 21$  independent<sup>8</sup> ensembles. The flow time discretization effects in the latter two strategies are expected<sup>9</sup> to be small.

Our Tab. 2 contains some metrics of the ensembles generated, like the number of measurements made and the number of update packages between adjacent measurements. An update package consists of a heatbath sweep [30–33] followed by four overrelaxation sweeps [34–36]. Occasionally, a

<sup>7</sup>The quantity  $t_0$  has the dimension of an area (or inverse mass squared), hence the ratio  $\sqrt{t_0}/r_0$  is a real number which assumes a universal value in the continuum limit  $a \rightarrow 0$ .

<sup>8</sup>The original plan was to generate only five lattice spacings. At  $\beta = 6.0314, 6.1912$  a slight increase of  $\rho$  from 0.06 to  $\sim 0.061$  or from 0.12 to  $\sim 0.122$  was needed to fit in these lattices.

<sup>9</sup>Comparing the top-left and bottom-left panels in Fig. 13 of Ref. [23] we see no hint for any flow time discretization effects in  $\chi_{\text{top}}^{1/4} r_0$  at flow times and step sizes similar to ours.

$L/a$	$\beta$	$r_0/a$	$a$ [fm]	7 stout	flow 0.21 fm	flow 0.30 fm
12	5.9421	4.8420	0.101	$7 \times 0.12$	$9 \times 0.06 = 0.54$	$9 \times 0.12 = 1.08$
14	6.0314	5.6490	0.087	$7 \times 0.12$	$12 \times 0.06125 = 0.735$	$12 \times 0.1225 = 1.47$
16	6.1142	6.4560	0.076	$7 \times 0.12$	$16 \times 0.06 = 0.96$	$16 \times 0.12 = 1.92$
18	6.1912	7.2630	0.067	$7 \times 0.12$	$20 \times 0.06075 = 1.215$	$20 \times 0.1215 = 2.43$
20	6.2629	8.0700	0.061	$7 \times 0.12$	$25 \times 0.06 = 1.5$	$25 \times 0.12 = 3.00$
24	6.3929	9.6841	0.051	$7 \times 0.12$	$36 \times 0.06 = 2.16$	$36 \times 0.12 = 4.32$
28	6.5079	11.298	0.043	$7 \times 0.12$	$49 \times 0.06 = 2.94$	$49 \times 0.12 = 5.88$

Table 1: Overview of the box sizes and couplings selected for the continuum scaling analysis. The volume  $V = (2.4783 r_0)^4$  is fixed in physical units, based on  $r_0/a$  as given in Eq. (14) of Ref. [6]. The “7stout” smoothing strategy keeps the flow time in lattice units fixed at  $t/a^2 = 7 \times 0.12 = 0.84$ , tantamount to  $\sqrt{8t} = \sqrt{6.72} a \rightarrow 0$  in physical units for  $\beta \rightarrow \infty$ . The “flow 0.21 fm” strategy sets the flow time to  $t/a^2 = (N/4)^2 \times 0.06$ , tantamount to  $\sqrt{8\tau} = 0.429 r_0 \simeq 0.21$  fm. The “flow 0.30 fm” strategy sets the flow time to  $t/a^2 = (N/4)^2 \times 0.12$ , tantamount to  $\sqrt{8\tau} = 0.607 r_0 \simeq 0.30$  fm.

$L/a$	$\beta$	7 stout	flow 0.21 fm	flow 0.30 fm	7 stout	flow 0.21 fm	flow 0.30 fm
12	5.9421	100000[10]	100000[10]	100000[10]	0.650(10)	0.640(10)	0.660(10)
14	6.0314	209519[10]	200000[10]	200000[10]	1.120(20)	1.130(20)	1.150(20)
16	6.1142	40851[64]	50654[64]	49617[64]	0.570(10)	0.560(10)	0.550(10)
18	6.1912	54583[81]	54760[81]	54577[81]	0.720(20)	0.710(20)	0.730(20)
20	6.2629	78749[100]	83474[100]	106925[100]	1.020(2)	1.060(30)	1.030(20)
24	6.3929	93292[100]	56238[144]	69276[144]	3.08(10)	2.209(90)	2.280(80)
28	6.5079	68641[196]	126804[196]	87726[196]	4.81(24)	5.04(26)	5.34(28)

Table 2: Details of the ensembles used in the continuum extrapolation. Columns three to six contain the number of measurements and the number of update packages between adjacent measurements in the format  $n_{\text{meas}}[n_{\text{sepa}}]$ . A separate stream was generated for each smoothing strategy. The remaining three columns contain  $\tau_{\text{int}}(q_{\text{ren}}^2)$  where  $q_{\text{ren}}$  uses the smoothing strategy listed in the column head.

$P$ -transformation [37] of the gauge configuration is applied (this preserves the action and flips the sign of  $q_{\text{ren}}$ ). The last three columns give  $\tau_{\text{int}}(q_{\text{ren}}^2)$ , where  $q_{\text{ren}}$  uses the smoothing strategy listed in the column head.

The original (unsmear) plaquettes are displayed in the first panel of Fig. 1. In log-log representation versus  $a/r_0$  (or our  $a/L$ ) they appear almost linear. A marked difference between the “7 stout” smoothing strategy on the one hand and the “flow 0.21 fm”, “flow 0.30 fm” strategies on the other hand is illustrated in the second panel. With a fixed flow time in lattice units (“7 stout”) the slope in the log-log representation is small, while with a fixed flow time in physical units (“flow 0.21 fm”, “flow 0.30 fm”) it is much steeper. This is unsurprising, since with the latter two strategies the number of stout steps in Tab. 1 proliferates towards the continuum.

The last step missing is a non-perturbative determination of the renormalization factors  $Z_q(\beta)$ . Following Refs. [6, 22, 38, 39] we calculate, for each ensemble and smoothing strategy, the quantity

$$\chi_{\min}^2 = \min_{1 \leq Z \leq 2} \sum_{i=1}^{n_{\text{conf}}} \left( Z q_{\text{nai}}^{(i)} - \text{round}(Z q_{\text{nai}}^{(i)}) \right)^2 \quad (13)$$

and the  $Z$  which realizes the minimum is the global topological charge renormalization factor  $Z_q$

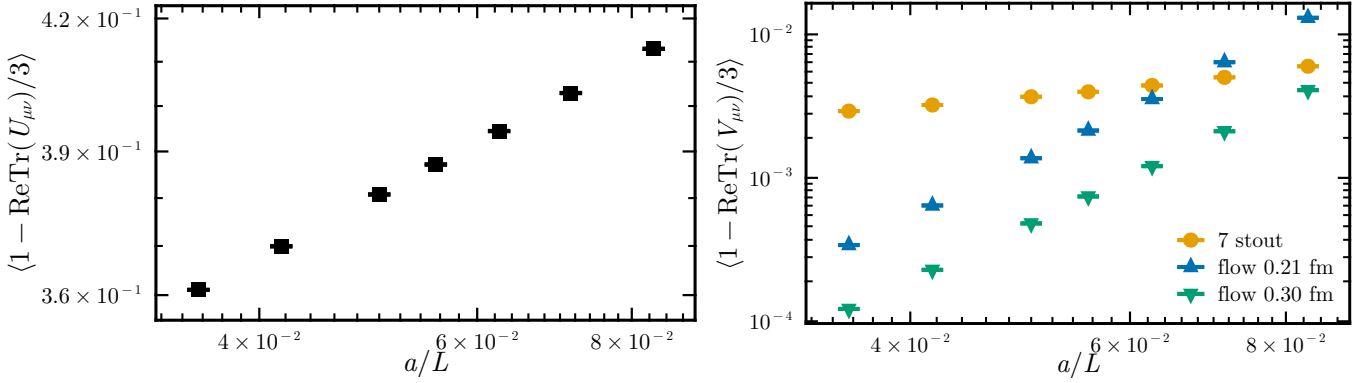


Figure 1:  $\langle 1 - \text{ReTr}(U_{\mu\nu})/3 \rangle$  of the ensembles used in the continuum extrapolation, unsmoothed (left) and with one of the three smoothing strategies (right).

$L/a$	$\beta$	7 stout	flow 0.21 fm	flow 0.30 fm
12	5.9421	1.2757(18)	1.3782(57)	1.2337(20)
14	6.0314	1.22881(57)	1.2522(12)	1.15821(41)
16	6.1142	1.1974(10)	1.17807(80)	1.11444(49)
18	6.1912	1.17499(62)	1.13280(43)	1.08579(26)
20	6.2629	1.15682(53)	1.10237(47)	1.06672(17)
24	6.3929	1.13312(31)	1.06700(16)	1.04426(11)
28	6.5079	1.11818(37)	1.04740(10)	1.03149(12)

Table 3: The multiplicative renormalization factor  $Z_q$  of the gluonic topological charge, determined for each smoothing strategy at various lattice spacings in a fixed physical volume  $V = (2.4783 r_0)^4$ .

(for the given  $\beta$  and the chosen smearing/flow recipe). The results are tabulated in Tab. 3 and displayed in Fig. 2. For each smoothing strategy the  $Z_q$  factor decreases towards the continuum. Plotting  $Z_q$  as a function of  $a^2$  (left panel) the function seems to pass through 1 at  $a = 0$  for the physical flow time strategies (“flow 0.21 fm”, “flow 0.30 fm”), even though these were unconstrained fits. If the flow time is fixed in lattice units (“7stout”), the extrapolation in  $(a/r_0)^2$  misses 1 in the continuum by many sigmas. The theoretically better motivated extrapolation in  $g_0^2 = 6/\beta$  is more cumbersome to fit (right panel). After some exercising we were successful with the ansatz  $Z_q = (1 + a_1/\beta + a_2/\beta^2)/(1 + b_1/\beta + b_2/\beta^2)$ . It results in dof = 7 – 4 = 3 and yields the  $P$  values 0.171, 0.896 and 0.350 for “7stout”, “flow 0.21 fm” and “flow 0.30 fm”, respectively.

## 4 Continuum analysis for the topological susceptibility

With these preparatory steps being taken, we are in a position to present the main analysis for the continuum extrapolation of the topological susceptibility.

The  $7 \times 3 = 21$  ensembles with a fixed physical volume are used to measure the naive topological charge (4) and (using the  $Z_q$  factor determined in Sec. 3) the renormalized charge (6). In either case the second moment of the distribution is determined, and the result is listed as  $q_{\text{nai}}^2$  (first three columns) and  $q_{\text{ren}}^2$  (last three columns) in Tab. 4. Given (7) and  $V = (2.4783 r_0)^4$ , these numbers must be divided by  $2.4783^4$  to obtain  $\chi_{\text{top}} r_0^4$ . All that remains to be done is to get rid of the discretization effects by means of a continuum extrapolation with  $O(a^2)$  cut-off effects.

First we discuss this extrapolation for the data based on  $q_{\text{ren}}^2$  (last three columns of Tab. 4), since

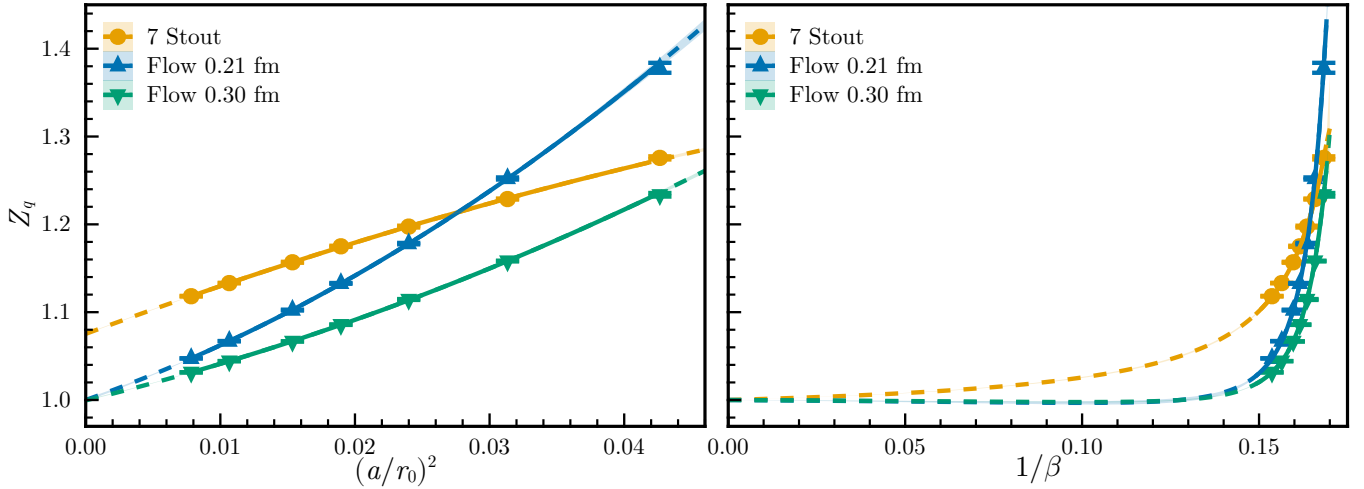


Figure 2: The  $Z_q$  factors involved, with quadratic fits in  $(a/r_0)^2$  (left) and rational fits in  $g_0^2$  (right).

$L/a$	$\beta$	7 stout	flow 0.21 fm	flow 0.30 fm	7 stout	flow 0.21 fm	flow 0.30 fm
12	5.9421	1.4653(78)	1.2158(64)	1.5970(85)	2.453(12)	2.387(12)	2.486(13)
14	6.0314	1.5362(74)	1.4734(73)	1.7419(88)	2.369(11)	2.364(12)	2.365(12)
16	6.1142	1.554(12)	1.633(11)	1.806(11)	2.268(17)	2.294(14)	2.254(14)
18	6.1912	1.592(12)	1.715(13)	1.871(14)	2.222(17)	2.214(16)	2.212(17)
20	6.2629	1.619(12)	1.781(13)	1.897(12)	2.185(16)	2.171(16)	2.162(14)
24	6.3929	1.617(19)	1.834(24)	1.899(22)	2.088(25)	2.090(27)	2.072(24)
28	6.5079	1.627(28)	1.847(24)	1.926(32)	2.046(35)	2.027(26)	2.050(34)

Table 4: Ensemble average and statistical error of  $q_{\text{nai}}^2$  (first three data columns) and  $q_{\text{ren}}^2$  (last three columns), as determined for each smoothing strategy and lattice spacing in the fixed physical volume  $V = (2.4783 r_0)^4$ . These results reflect  $7 \times 3$  different ensembles.

this is the standard procedure [6, 20–23]. We obtain good fits with a “const+linear” fit (in  $a^2$ ) that excludes the coarsest ( $\beta = 5.9421$ ) lattice spacing, and with a “const+linear+quadratic” fit that includes all spacings. The results are presented in Fig. 3. The extrapolated values at  $a = 0$  for the three smoothing strategies are completely independent (as are the ensembles). With the linear ansatz they agree very closely, with the quadratic ansatz (in  $a^2$ ) there is a visible spread, but they still agree within (statistical) errors. Extrapolating  $\chi_{\text{top}} r_0^4$  is not the only possibility, also  $\chi_{\text{top}}^{1/2} r_0^2$  or  $\chi_{\text{top}}^{1/4} r_0$  are permissible. We add the latter option to control the pertinent systematics; the results are shown in Fig. 4. Again “const+linear” without the coarsest lattice spacing and “const+linear+quadratic” with all data included are found to yield acceptable fits.

At this point we have four valid continuum extrapolations of the topological susceptibility (or its fourth root) for each one of the three smoothing strategies. These results are shown in Tab. 5. Note that for each smoothing strategy (e.g. “7stout”) the four entries describe a joint continuum limit (their spread indicates a systematic uncertainty). There is, however, no guarantee that the “ultralocal” strategy (“7stout”) and either one of the “fixed physical flow time” strategies (“flow 0.21 fm” and “flow 0.30 fm”) would yield the same continuum limit. As mentioned in Sec. 3, the latter two strategies introduce a second regulator which persists in the continuum limit, and it is the claim of Ref. [29] that this second regulator leaves the continuum value of  $\chi_{\text{top}}^{1/4} r_0$  unaffected. We are thus

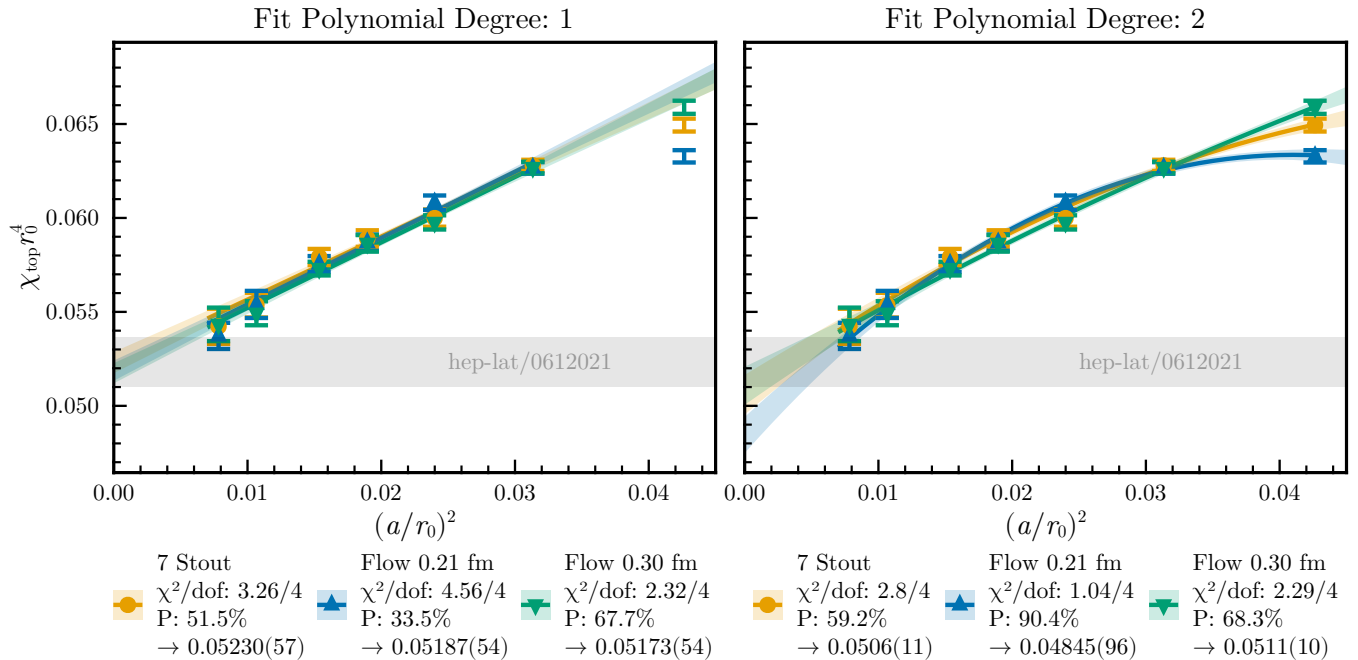


Figure 3: Continuum extrapolation of the topological susceptibility with an ansatz linear in  $a^2$  based on the six finest spacings (left) and with an ansatz quadratic in  $a^2$  based on all seven spacings (right).

	$[\chi_{\text{top}} r_0^4]_{\text{lin.}}$	$[\chi_{\text{top}} r_0^4]_{\text{quad.}}$	$[\chi_{\text{top}}^{1/4} r_0]_{\text{lin.}}$	$[\chi_{\text{top}}^{1/4} r_0]_{\text{quad.}}$
7 stout	0.05230(57)	0.0506(11)	0.4789(12)	0.4749(22)
flow 0.21 fm	0.05187(54)	0.04845(96)	0.4780(12)	0.4703(21)
flow 0.30 fm	0.05173(54)	0.0511(10)	0.4777(11)	0.4757(22)

Table 5: Continuum value, at fixed physical volume  $V = (2.4783 r_0)^4$ , of either  $\chi_{\text{top}} r_0^4$  or its fourth root, as extracted with one of two fitting ansätze and one of three smearing strategies. The statistical errors along each line are highly correlated, but fully uncorrelated along each column.

left with the task to condense, for each smoothing strategy, the four entries in Tab. 5 into a single number (with a statistical and a systematic uncertainty). With these final numbers in hand (one for “7 stout”, “flow 0.21 fm” and “flow 0.30 fm” each) we will be able to put the claim to a test.

We will proceed in two steps (first we combine the two fit ansätze, then the two ordering options of the fourth root and the extrapolation). For the first line of Tab. 5 this means that we combine  $0.05230(57)_{\text{stat}}$  and  $0.0506(11)_{\text{stat}}$  to become  $0.05194(68)_{\text{stat}}$ , where the average of the statistical errors was done with the same weights that were used for the average of the central values, since these errors are highly correlated. In addition, the combined value needs to be attributed a systematic uncertainty to reflect the spread between the two numbers from which it was derived. On this point we follow Refs. [40, 41] which recommend using

$$\sigma_{\text{sys}} = |c^{(1)} - c^{(2)}| \operatorname{erf} \left( \frac{|c^{(1)} - c^{(2)}|}{\sqrt{2} \max(\sigma_{\text{stat}}^{(1)}, \sigma_{\text{stat}}^{(2)})} \right) \quad (14)$$

for combining two central values  $c^{(1)}, c^{(2)}$  with statistical uncertainties  $\sigma_{\text{stat}}^{(1)}, \sigma_{\text{stat}}^{(2)}$ , since this is the difference between the continuum extrapolations obtained from the two fitting ansätze, multiplied by the



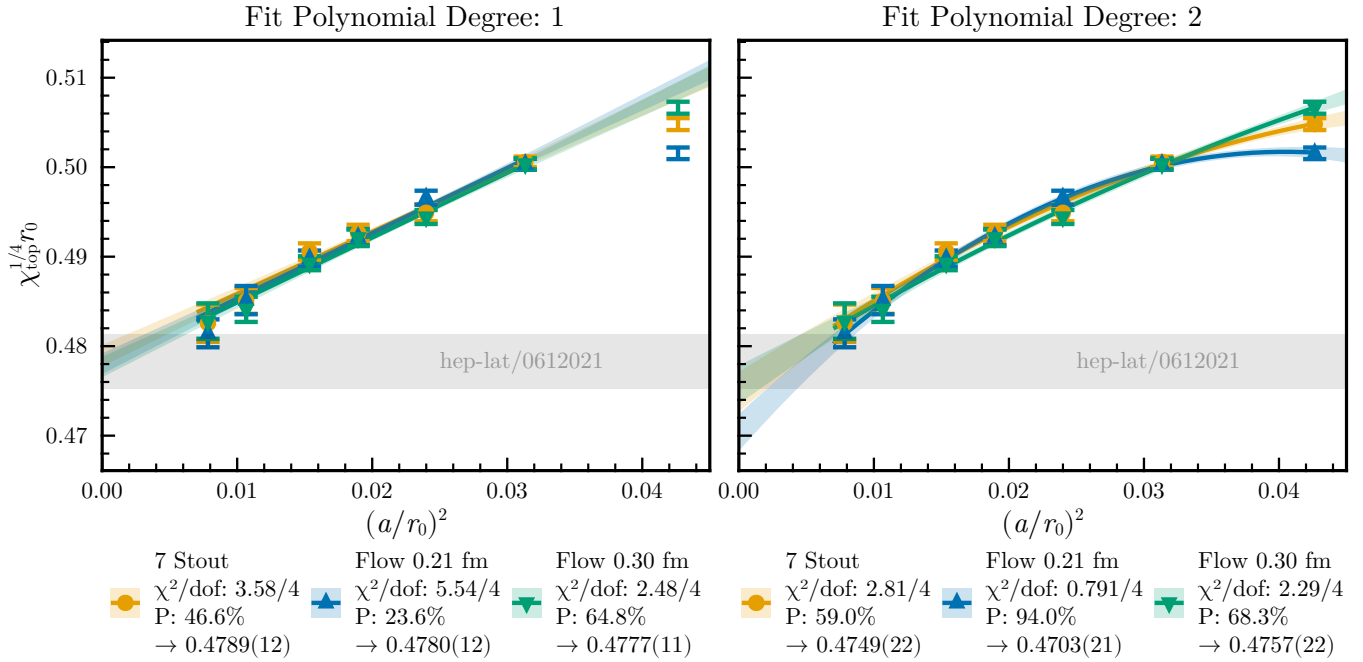


Figure 4: Same as Fig. 3 but with the quantity  $\chi_{\text{top}}^{1/4} r_0$  on the ordinate (and six freshly created fits).

	$\chi_{\text{top}} r_0^4$	$\chi_{\text{top}}^{1/4} r_0$	combined
7 stout	0.05194(68)(149)=[0.4774(16)(34)] <sup>4</sup>	0.4780(14)(37)	0.4776(15)(35)(01)
flow 0.21 fm	0.05105(64)(342)=[0.4753(15)(80)] <sup>4</sup>	0.4761(14)(77)	0.4759(15)(79)(01)
flow 0.30 fm	0.05159(64)(030)=[0.4766(15)(07)] <sup>4</sup>	0.4773(13)(13)	0.4769(14)(10)(03)

Table 6: Results of the continuum extrapolation of  $\chi_{\text{top}} r_0^4$  (left column) or  $\chi_{\text{top}}^{1/4} r_0$  (middle column).

probability that this difference is due to a statistical fluctuation. For the “7 stout” strategy this yields  $0.05194(68)_{\text{stat}}(149)_{\text{sys}}$  as the continuum limit of  $\chi_{\text{top}} r_0^4$ , and similarly one finds  $0.4780(14)_{\text{stat}}(37)_{\text{sys}}$  for the continuum limit of  $\chi_{\text{top}}^{1/4} r_0$ . Finally, these two figures may be combined with the help of (14) to yield  $0.4776(15)_{\text{stat}}(35)_{\text{sys}}(01)_{\text{sys}}$ . This number is stored in Tab. 6, together with similar numbers for the “flow 0.21 fm” and “flow 0.30 fm” strategies. Evidently, these three figures are consistent within (overall) errors, in agreement with the claim of Ref. [29].

Finally, we like to point out that our observation that exclusively for a “fixed physical flow time” strategy the  $Z_q$ -factor is of the form  $Z_q \simeq 1 + \text{const} \cdot a^2 + \text{const} \cdot a^4$  (see Fig. 2) allows for a non-standard continuum extrapolation of the topological susceptibility in such a strategy. Hence, the data based on  $q_{\text{nai}}^2$  (first three columns of Tab. 4) can be extrapolated without any further renormalization, but only for the “flow 0.21 fm” and “flow 0.30 fm” columns, not for the “7 stout” column. For  $\chi_{\text{top}} r_0^4$  this is shown in Fig. 5, while a similar plot for  $\chi_{\text{top}}^{1/4} r_0$  is suppressed for brevity. The open up (down) triangles yield the same continuum limit as the full up (down) triangles. The statistical error in the continuum is even smaller than with the standard extrapolation; this suggests that our results in Tab. 6 come with conservatively assessed systematics. For the “7 stout” strategy, on the other hand, the continuum limit of  $q_{\text{nai}}^2$  is visibly different from the one of  $q_{\text{ren}}^2$ , in agreement with the observation made in Fig. 2 that this  $Z_q$ -factor follows a different path towards the continuum.

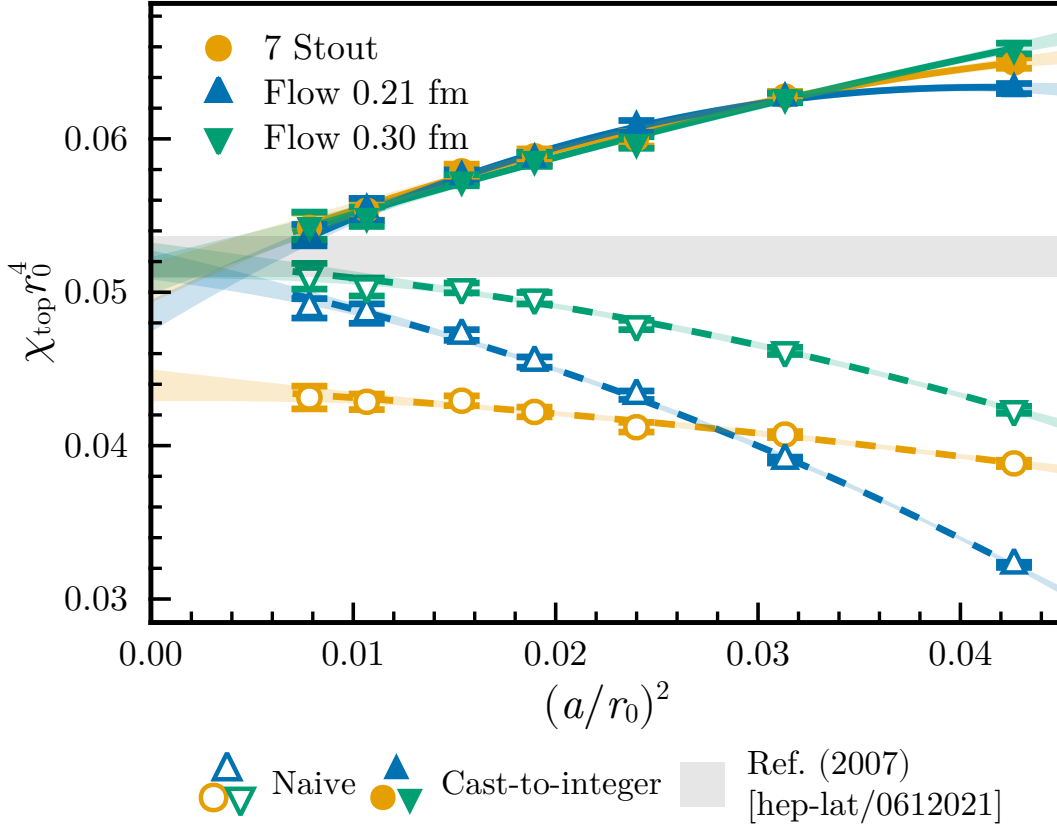


Figure 5: *The standard continuum extrapolation as presented in the right panel of Fig. 3 (full symbols) compared to a non-standard approach where the  $Z_q$ -factor and the cast-to-integer operation are omitted (open symbols). In both cases the data for all three smearing strategies are shown.*

To summarize this section, we recall the final results with the three smoothing strategies

$$[\chi_{\text{top}}^{1/4} r_0]_{7 \text{ stout}} = 0.4776(15)_{\text{stat}}(35)_{\text{syst}} = 0.4776(38)_{\text{tot}} \quad (15)$$

$$[\chi_{\text{top}}^{1/4} r_0]_{0.21 \text{ fm}} = 0.4759(15)_{\text{stat}}(79)_{\text{syst}} = 0.4759(80)_{\text{tot}} \quad (16)$$

$$[\chi_{\text{top}}^{1/4} r_0]_{0.30 \text{ fm}} = 0.4769(14)_{\text{stat}}(11)_{\text{syst}} = 0.4769(18)_{\text{tot}} \quad (17)$$

from Tab. 6 and note that they seem perfectly consistent, hence supporting the claim of Ref. [29]. In view of this, we may select the result of the “0.30 fm” strategy as our final result (or average over the three strategies, it hardly makes any difference). In physical units we thus obtain

$$\chi_{\text{top}}^{1/4} = \frac{0.4769(18)}{0.4757(64) \text{ fm}} = 197.8(0.7)(2.7) \text{ MeV} \quad (18)$$

where the first bracket gives the combined (statistical and systematic errors added in quadrature) uncertainty of our calculation, and the second one the uncertainty of  $r_0$  as taken from Ref. [42]. The 0.4% uncertainty of  $\chi_{\text{top}}^{1/4} r_0$  (or 1.5% uncertainty of  $\chi_{\text{top}} r_0^4$ ) will be put into context in Sec. 7.

## 5 Continuum analysis for the topological excess kurtosis

The measured distribution of  $q_{\text{ren}}$  is, for each  $\beta$ , precise enough that we can attempt to determine a fourth-order cumulant (with a subsequent continuum limit). For a random variable  $X$  with mean  $\mu$

$L/a$	$\langle q_{\text{ren}}^4 \rangle / \langle q_{\text{ren}}^2 \rangle^2 - 3$	$\langle q_{\text{ren}}^4 \rangle / \langle q_{\text{ren}}^2 \rangle - 3 \langle q_{\text{ren}}^2 \rangle$	$\langle q_{\text{ren}}^4 \rangle - 3 \langle q_{\text{ren}}^2 \rangle^2$
12	0.135(20),0.088(18),0.129(18)	0.331(48),0.209(43),0.320(45)	0.81(12), 0.50(10), 0.80(11)
14	0.105(14),0.111(15),0.131(15)	0.249(33),0.262(34),0.310(35)	0.590(78), 0.620(82), 0.733(84)
16	0.098(29),0.138(21),0.116(20)	0.221(65),0.317(49),0.261(44)	0.50(15), 0.73(11), 0.587(100)
18	0.119(25),0.093(24),0.130(25)	0.265(56),0.205(52),0.287(56)	0.59(13), 0.45(12), 0.64(12)
20	0.127(22),0.148(24),0.131(19)	0.277(48),0.320(52),0.283(41)	0.61(10), 0.69(11), 0.612(90)
24	0.131(34),0.136(35),0.075(32)	0.273(71),0.283(73),0.155(67)	0.57(15), 0.59(15), 0.32(14)
28	0.112(47),0.157(36),0.249(48)	0.229(96),0.318(74),0.51(10)	0.47(20), 0.64(15), 1.03(21)

Table 7: *Ensemble average and statistical error of the excess kurtosis varieties on all ensembles in a physical volume  $V = (2.4783 r_0)^4$ . Results for the “7stout”, “flow 0.21 fm” and “flow 0.30 fm” smoothing strategies are comma separated in each cell. For  $\beta = \beta(L/a)$  see Tab. 4.*

and variance  $\sigma^2$ , the “standard kurtosis” is defined as  $\langle Y^4 \rangle$ , where  $Y = (X - \mu)/\sigma$ . If  $X$  is Gaussian, then  $\langle Y^2 \rangle = 1$  and  $\langle Y^4 \rangle = 3$ . Therefore one defines the “excess kurtosis” of  $X$  as  $\langle Y^4 \rangle / \langle Y^2 \rangle^2 - 3$  or  $\langle Y^4 \rangle / \langle Y^2 \rangle - 3 \langle Y^2 \rangle$  or  $\langle Y^4 \rangle - 3 \langle Y^2 \rangle^2$ ; each one of these quantities is zero for a Gaussian  $X$ .

We measured these four varieties of the excess kurtosis of  $q_{\text{ren}}$  for all our ensembles, the results are given in Tab. 7. The “7stout”, “flow 0.21 fm” and “flow 0.30 fm” results are given as a comma separated list in each cell. These results are also displayed in Fig. 6; it seems that the data approach a well-defined continuum limit. Upon dropping the coarsest (and for the “flow 0.30 fm” strategy also the finest) lattice spacing, we get good fits with a single constant for each smearing strategy. The continuum limit in the fixed physical volume  $V = (2.4783 r_0)^4$  is found to be

$$\langle q_{\text{ren}}^4 \rangle / \langle q_{\text{ren}}^2 \rangle^2 - 3 = 0.1126(94)_{7\text{stout}}, \quad 0.1232(91)_{\text{flow } 0.21 \text{ fm}}, \quad 0.1235(90)_{\text{flow } 0.30 \text{ fm}} \quad (19)$$

$$\langle q_{\text{ren}}^4 \rangle / \langle q_{\text{ren}}^2 \rangle - 3 \langle q_{\text{ren}}^2 \rangle = 0.255(21)_{7\text{stout}}, \quad 0.278(21)_{\text{flow } 0.21 \text{ fm}}, \quad 0.276(20)_{\text{flow } 0.30 \text{ fm}} \quad (20)$$

$$\langle q_{\text{ren}}^4 \rangle - 3 \langle q_{\text{ren}}^2 \rangle^2 = 0.574(48)_{7\text{stout}}, \quad 0.622(46)_{\text{flow } 0.21 \text{ fm}}, \quad 0.614(45)_{\text{flow } 0.30 \text{ fm}} \quad (21)$$

and one should keep in mind that the panels in Fig. 6 are vertically correlated but not horizontally (we have a separate ensemble for each smoothing strategy).

Regardless which definition of the excess kurtosis is chosen, it is striking to the eye that the horizontal bands of the three smoothing strategies in Fig. 6 are consistent within errors. This is consistent with what we saw for the second moment (compare Tab. 6). We feel tempted to speculate that the claim of Ref. [29] could be extended to say that any moment<sup>10</sup> of the  $q_{\text{ren}}$  distribution in a fixed physical volume has a well defined continuum limit which does not depend on whether a “fixed  $t/a^2$ ” or a “fixed  $t/r_0^2$ ” smoothing strategy was chosen.

We should keep in mind, however, that both the final results (15-17) of Sec. 4 and the final results (19-21) of this section are subject to potential finite-volume artefacts.

## 6 Infinite volume extrapolation

To get rid of potential finite volume effects in the continuum results obtained in Secs. 4 and 5 we need data with different box sizes  $L$ . In a gapped theory these finite-volume effects scale like [43]

$$\chi_{\text{top}}(L) = \chi_{\text{top}}(\infty) \cdot [1 + \text{const } e^{-M_G L}] \quad (22)$$

where  $M_G$  is the mass of a glueball state in the YM theory. The finite-volume effects represent small corrections due to IR physics; it is thus justified to study them at a single lattice spacing.

<sup>10</sup>This is equivalent to the statement that the  $q_{\text{ren}}$  distribution in a fixed physical volume has this property.

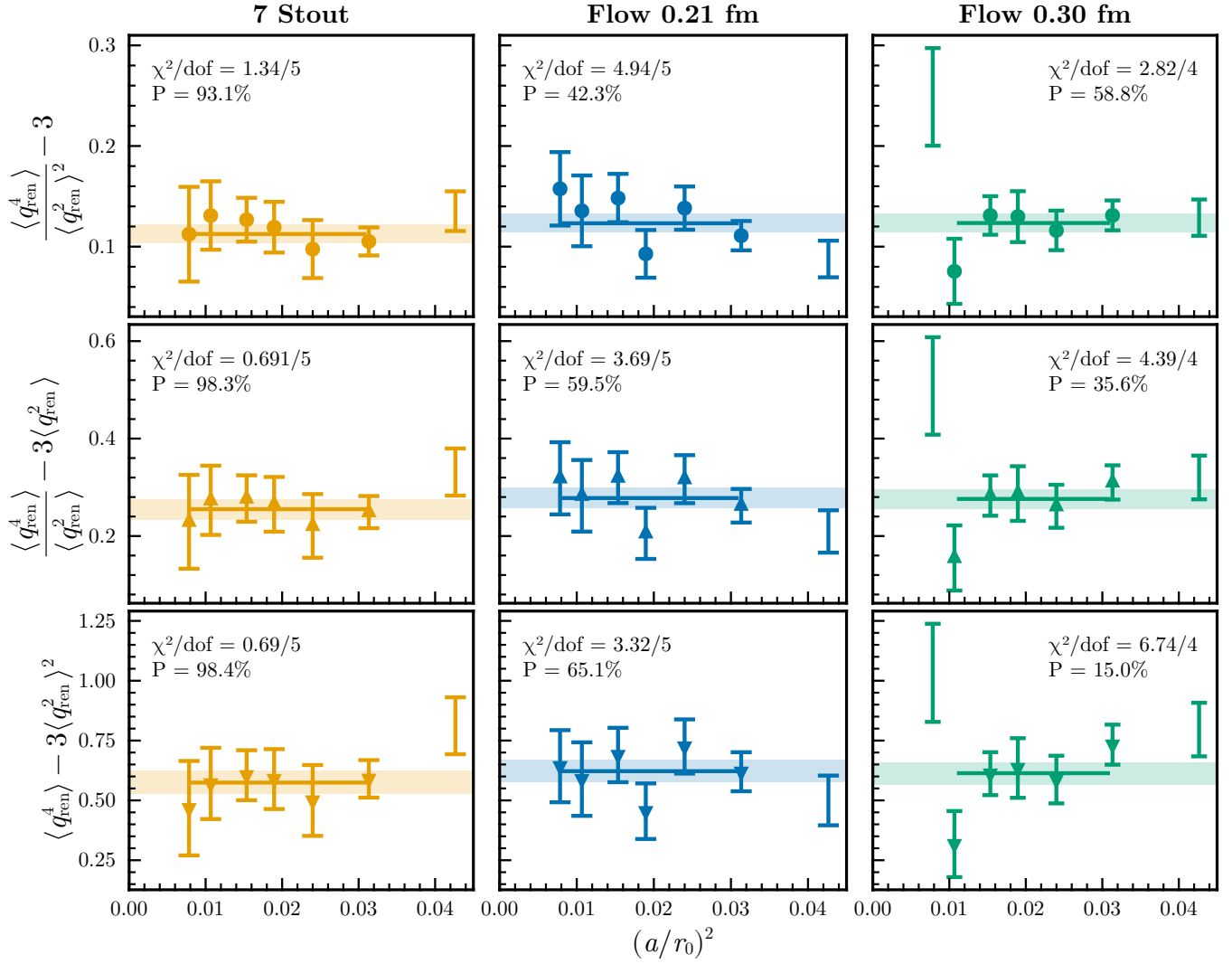


Figure 6: Continuum extrapolation of three varieties of the excess kurtosis (top, middle, bottom) for our three smearing strategies (“7 stout” left, “flow 0.21 fm” middle, “flow 0.30 fm” right).

We select our intermediate coupling ( $\beta = 6.1912$ ,  $18^4$  lattice) of the continuum series, and augment it with smaller/larger boxes as indicated in Tab. 8. We do fewer updates between adjacent measurements [to establish  $\tau_{\text{int}}(q_{\text{ren}}^2) \simeq 1$ ] and (over)compensate this by a larger number of measurements. Since potential finite volume effects originate in the IR physics of the original (unsmeared) gauge configuration, it is sufficient to do this for one smoothing strategy (we select the “7 stout” strategy). We expect that the factor  $Z_q$  in the definition (6) of  $q_{\text{ren}}$  is essentially independent of  $L/r_0$ , unless the box volume is so small that deconfinement effects are present. Indeed, the last column of Tab. 8 confirms this expectation, but the errors grow with the volume. Therefore we follow Ref. [6] and use, in the analysis below, the value  $Z_q = 1.17499(62)$  of the  $18^4$  box for all volumes.

With these preparatory steps taken, we determine the second and fourth moment<sup>11</sup> of the  $q_{\text{ren}}$  distribution on the ensembles mentioned. For the latter moment we measure the same three varieties of the excess kurtosis that were studied in Sec. 5. The results are listed in Tab. 9.

The first data column of this table is easy to interpret. The quantity  $\langle q_{\text{ren}}^2 \rangle$  grows linearly with the volume  $V$ , so  $\chi_{\text{top}} = \langle q_{\text{ren}}^2 \rangle / V$  assumes a finite value in the limit  $V \rightarrow \infty$ , in agreement with

<sup>11</sup>We checked that  $\langle q_{\text{ren}} \rangle$  and  $\langle q_{\text{ren}}^3 \rangle$  are zero within errors.

$L/a$	$\beta$	$n_{\text{meas}}[n_{\text{sepa}}]$	$\tau_{\text{int}}(q_{\text{ren}}^2)$	$Z_q$ (7 stout)
12	6.1912	200000[50]	1.117(17)	1.18218(64)
14	6.1912	200000[50]	1.133(18)	1.17604(35)
16	6.1912	212789[50]	1.036(19)	1.17378(52)
18	6.1912	54583[81]	0.721(17)	1.17499(62)
20	6.1912	204997[50]	1.010(27)	1.17282(39)
24	6.1912	324894[50]	1.045(37)	1.17292(58)
28	6.1912	246512[50]	1.056(51)	1.1717(16)

Table 8: *Details of the ensembles used in the infinite volume extrapolation. The format is the same as in Tabs. 2 and 3, except that this time we restrict ourselves to the “7stout” strategy.*

$L/a$	$\beta$	$\langle q_{\text{ren}}^2 \rangle$	$\langle q_{\text{ren}}^4 \rangle / \langle q_{\text{ren}}^2 \rangle^2 - 3$	$\langle q_{\text{ren}}^4 \rangle / \langle q_{\text{ren}}^2 \rangle - 3\langle q_{\text{ren}}^2 \rangle$	$\langle q_{\text{ren}}^4 \rangle - 3\langle q_{\text{ren}}^2 \rangle^2$
12	6.1912	0.1911(17)	4.998(79)	0.956(14)	0.1827(34)
14	6.1912	0.6689(38)	0.897(26)	0.600(18)	0.401(12)
16	6.1912	1.3482(63)	0.238(15)	0.320(20)	0.432(27)
18	6.1912	2.222(17)	0.119(25)	0.265(56)	0.59(12)
20	6.1912	3.394(15)	0.053(13)	0.181(43)	0.61(14)
24	6.1912	7.019(25)	0.045(11)	0.318(74)	2.24(52)
28	6.1912	13.050(53)	0.005(11)	0.06(14)	0.8(1.8)

Table 9: *Ensemble average and statistical error of the squared topological charge and the three kurtosis varieties for the ensembles listed in Tab. 8. Throughout the “7stout” strategy is used.*

theory [8]. This is illustrated in Fig. 7 where the topological susceptibility is plotted versus  $1/L$  and  $1/V$ . It seems that the standard volume used in Sec. 4 (marked with a dashed vertical line) is just large enough to avoid finite size effects (within the statistical precision that we have). Our final value (18) for  $\chi_{\text{top}}^{1/4}$  in physical units thus needs no further extrapolation.

The last three columns of Tab. 9 are not-so-easy to interpret. The  $\langle q_{\text{ren}}^4 \rangle / \langle q_{\text{ren}}^2 \rangle^2 - 3$  variety of the excess kurtosis definitely decreases with the box volume  $V$ , the  $\langle q_{\text{ren}}^4 \rangle / \langle q_{\text{ren}}^2 \rangle - 3\langle q_{\text{ren}}^2 \rangle$  variety seems somewhat undecided, and the  $\langle q_{\text{ren}}^4 \rangle - 3\langle q_{\text{ren}}^2 \rangle^2$  variety likely increases towards the largest volumes. Hence, we include a factor  $(L/r_0)^4$  in the first case, a factor 1 in the second case, and a factor  $(r_0/L)^4$  in the third case before plotting them in the left panels of Fig. 8. The striking observation is that – with these volume factors included – the data for the three varieties (without any fit) look similar to each other, except for a change in the vertical scale. In all cases we get a reasonable fit to a constant, if we include the four largest box volumes (shown).

However, it is by no means clear that the large-volume asymptotics of these quantities is a finite constant. In App. A we will present our hypothesis that one must include a factor  $(L/r_0)^2$ ,  $(r_0/L)^2$  and  $(r_0/L)^6$  for these quantities, respectively, in order to obtain a finite value in the infinite volume limit. The right panels of Fig. 8 give the reader a preview of how this hypothesis works on the present data. Again, the three excess kurtosis varieties are found to look similar to each other, except for a change in the overall scale. Each one of the right panels includes a fit of the largest four volumes to a constant, which (by the  $P$ -value) is worse than the respective fit in the left panel.

For now we can only say that the present data are insufficient to decide on the scaling exponent  $\alpha$  of the asymptotic behavior  $c(L/r_0)^\alpha$  for the quantities  $\langle q_{\text{ren}}^4 \rangle / \langle q_{\text{ren}}^2 \rangle^2 - 3$ ,  $\langle q_{\text{ren}}^4 \rangle / \langle q_{\text{ren}}^2 \rangle - 3\langle q_{\text{ren}}^2 \rangle$ , and  $\langle q_{\text{ren}}^4 \rangle - 3\langle q_{\text{ren}}^2 \rangle^2$ . This is why we decided to generate another data set to investigate the situation in

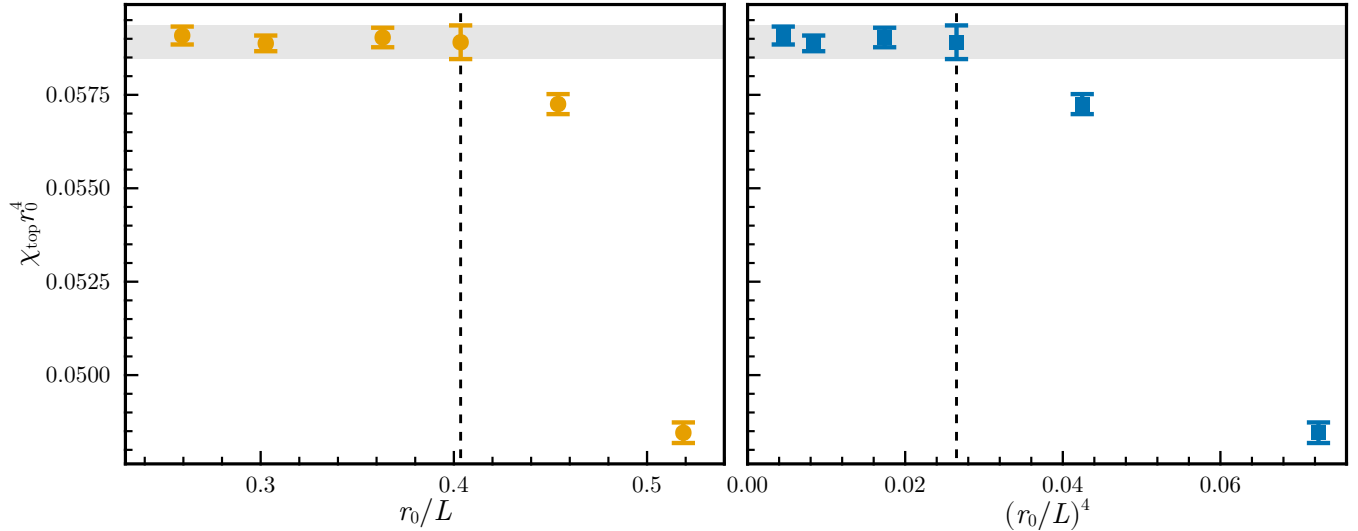


Figure 7: Volume scaling of the topological susceptibility plotted versus  $1/L$  (left) and  $1/V$  (right). The standard inverse size/volume used in Sec. 4 is marked with a dashed vertical line. The runs of Ref. [6] were performed with a box size  $\sim 10\%$  smaller, which coincides roughly with the fifth data point. The seventh data point is out of scale (both horizontally and vertically).

more detail (see App. A). As we shall see, the new data suggest the scaling exponents  $\alpha = -2, 2$  and  $6$  for these excess kurtosis varieties. In retrospect we will say that the volumes considered in the present section are large enough to reach definite conclusions for the large volume behavior of  $\langle q_{\text{ren}}^2 \rangle$ , but not for the three excess kurtosis varieties.

## 7 Summary and outlook

In this work we generated  $3 \times 7 + 6 + 6$  ensembles in  $SU(3)$  YM theory to determine the second and fourth moment of the topological charge distribution. From the second moment  $\langle q_{\text{ren}}^2 \rangle$  the topological susceptibility (7) was derived, while the fourth moment  $\langle q_{\text{ren}}^4 \rangle$  served to form the three varieties (19–21) of the excess kurtosis. The  $3 \times 7$  ensembles specified in Tab. 2 were used to obtain independent continuum extrapolations for three different smoothing strategies, dubbed “7 stout”, “flow 0.21 fm”, and “flow 0.30 fm”, respectively. The 6 ensembles in Tab. 8 proved sufficient to show the absence of finite volume effects in the topological susceptibility, while the 6 ensembles in Tab. 11 gave us confidence to conjecture the scaling laws (24) for the excess kurtosis.

Our final result for  $\chi_{\text{top}}^{1/4} r_0$  is given in Eq. (18), and repeated (along with its fourth power) in Tab. 10. This table also contains a selection of continuum extrapolated results from the literature. Except for Ref. [44] all these papers effectively compute  $\chi_{\text{top}}^{1/4} r_0$  or  $\chi_{\text{top}} r_0^4$ . This is why we ignore their final quote in physical units (if given) and convert, in the last column, all results with the same factor to MeV units. This factor  $r_0^{-1} = 414.8(5.6)$  MeV is taken from Ref. [42]; its error bar is reflected by the last parentheses (which dominates the final uncertainty).

Focusing on the  $\chi_{\text{top}}^{1/4} r_0$  column of Tab. 10, there is a slight tension between our result and Refs. [44–47] at the level of 3.1, 1.6, 2.5 and 1.5 combined standard deviations, respectively. On the other hand our result agrees with Ref. [29], Ref. [39] and Ref. [6] within 0.3, 0.8 and 0.5 combined standard deviations, respectively. Given the non-zero curvature in our Figs. 3 and 4, we can only speculate that with just three or four lattice spacings [44–47] it may be difficult to reliably assess the systematic uncertainty of the continuum extrapolated result. We have seven lattice spacings available, and we

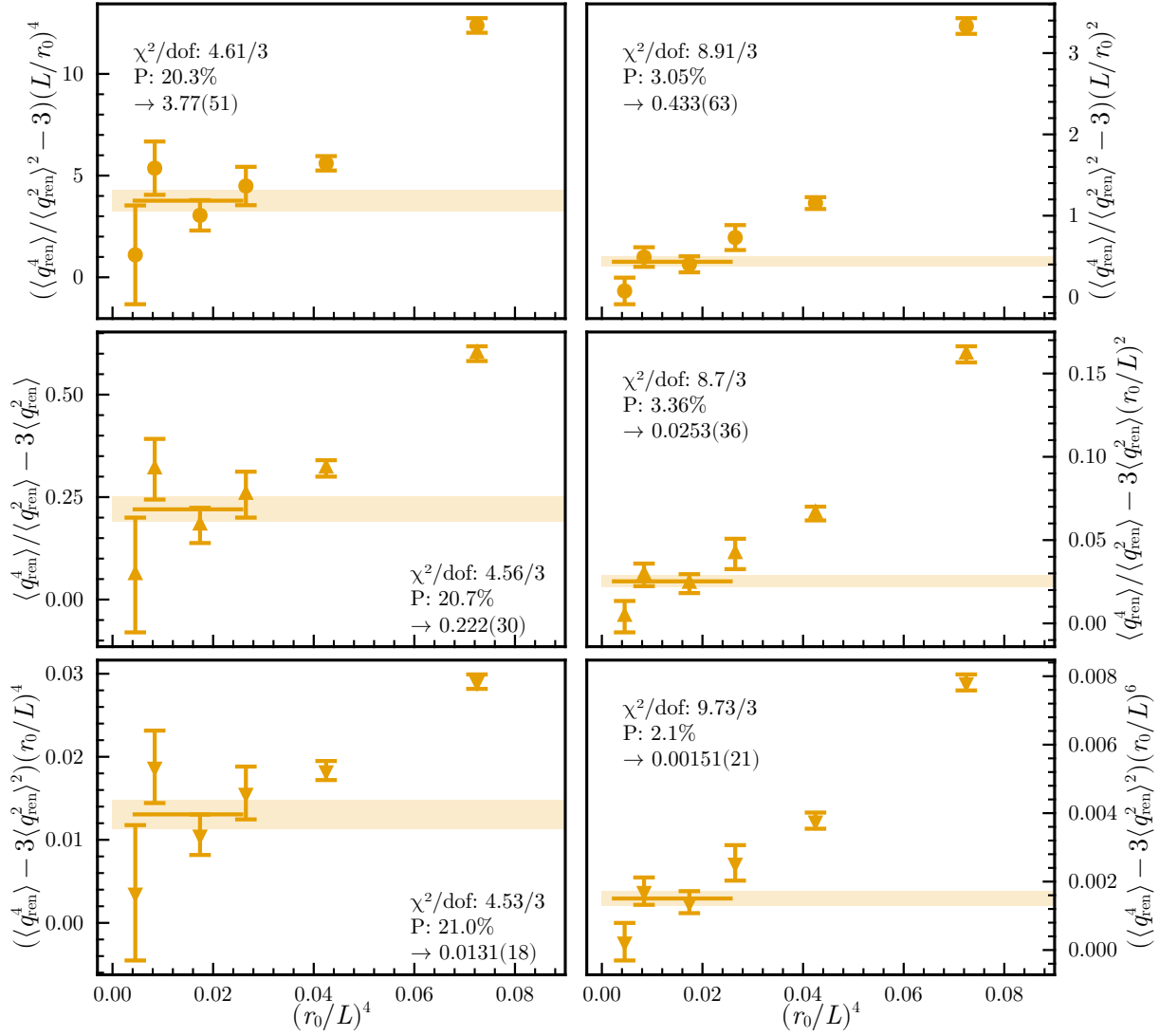


Figure 8: Large volume behavior of the three kurtosis varieties with the “7stout” smoothing strategy. In the left panel one variety is multiplied with  $(L/r_0)^4$ , one unchanged, one divided by  $(L/r_0)^4$  (top, middle, bottom). In the right panel the respective factors are  $(L/r_0)^2$ ,  $(r_0/L)^2$  and  $(r_0/L)^6$ .

use a large variety of fit functions and cuts to determine the systematic uncertainty.

Our standard volume  $V = L^4$  with  $L = 2.4783 r_0 = 1.179(16)$  fm gave a finite continuum limit of the excess kurtosis of the topological susceptibility, but our standard volume scaling lattices proved insufficient to determine the pertinent volume scaling laws. To this aim we generated a series of extra lattices (at a fixed coupling  $\beta = 5.9421$ ), ranging out to  $L_{\max} = 4.5436 r_0 = 2.161(29)$  fm. These data let us conjecture the large volume scaling laws (24) which, in turn, suggest that the quantities (25) yield finite values in the limit  $L \rightarrow \infty$ ; our values are quoted in the text ahead of Eq. (23).

Apart from addressing the excess kurtosis varieties (19-21), our work differs from previous investigations [44–47] by considering a constant flow-time in physical units (dubbed “flow 0.21 fm”, and “flow 0.30 fm”) in addition to the more traditional constant flow-time in lattice units (dubbed “7stout”). The former strategy realizes a universal renormalization scheme with a diffusion based scale which persists in the limit  $a \rightarrow 0$ , see the discussion in Sec. 2 and in Refs. [3, 4, 28]. The latter strategy links the flow scale to the lattice cutoff; in this case the flow regulator is removed upon letting  $a \rightarrow 0$ . It seems remarkable that the topological susceptibility would assume a joint

	$\chi_{\text{top}}^{1/4}/\sqrt{\sigma}$	$\chi_{\text{top}}^{1/4}r_0$	$\chi_{\text{top}}r_0^4$	$\chi_{\text{top}}^{1/4}$ [MeV]
this work (2025)	-	0.4769(18)	0.05173(78)	197.8(0.7)(2.7)
Ref. [29] (2023)	-	0.4794(86)	0.0528(38)	198.9(3.6)(2.7)
Ref. [44] (2021)	0.4246(36)	0.4926(48)	0.0589(23)	204.3(2.0)(2.8)
Ref. [39] (2015)	-	0.4708(72)	0.0491(30)	195.3(3.0)(2.7)
Ref. [45] (2010)	-	0.498(13)	0.0615(64)	206.6(5.4)(2.8)
Ref. [6] (2006)	-	0.4784(21)	0.05236(94)	198.4(0.9)(2.7)
Ref. [46] (2004)	-	0.4928(62)	0.059(3)	204.4(2.6)(2.8)
Ref. [47] (2003)	-	0.4928(104)	0.059(5)	204.4(4.3)(2.8)

Table 10: Comparison of  $\chi_{\text{top}}$  values in  $SU(3)$  gauge theory in the literature with continuum extrapolation, in units of  $r_0^{-4}$ . Results in units of  $\sqrt{\sigma}$  are converted on the basis of  $r_0\sqrt{\sigma} = 1.160(6)$  [44]. All values in the second column are converted to MeV by means of  $r_0 = 0.4757(64)$  fm [42].

$L/a$	$\beta$	$n_{\text{meas}}[n_{\text{sepa}}]$	$\tau_{\text{int}}(q_{\text{ren}}^2)$	$Z_q$ (7 stout)
10	5.9421	281979[10]	0.7039(76)	1.28139(96)
12	5.9421	100000[10]	0.653(11)	1.2757(18)
14	5.9421	535206[10]	0.6533(48)	1.2757(79)
16	5.9421	371035[10]	0.6485(67)	1.279(59)
18	5.9421	420704[10]	0.6481(76)	1.13(32)
20	5.9421	707643[10]	0.6465(90)	1.201(12)
22	5.9421	809898[10]	0.6369(93)	1.27(62)

Table 11: Details of the post production ensembles; the format is the same as in Tab. 8.

continuum limit under the auspices of either strategy [29]. Despite the high precision (and the statistical independence of the ensembles used for the different strategies) our continuum extrapolated results are in perfect agreement with this assertion.

Evidently, the research reported here is a snapshot in the broader context of lattice gluodynamics. It would be interesting to follow Ref. [44] and include a larger selection of  $N_c$ , not just  $N_c = 3$ . Also quantities with non-zero virtuality would be interesting, such as  $d\chi/dq^2$  at  $q^2 = 0$  or the glueball mass extracted from the long distance behavior of  $q(x)q(0)$ , but such quantities require the local charge density, not just the global topological charge. On the technical level, perhaps an improved field-strength definition as advocated in Ref. [48] might be a useful addition.

## A Production of another large volume data set

In an attempt to improve on the large volume scaling of the excess kurtosis presented in Sec. 6, we decided to generate another series of lattices which would reach towards larger physical volumes. For the intermediate coupling  $\beta = 6.1912$ , as used in that section, we exhausted our computational resources. Hence, another attempt must use a lower  $\beta$  (stronger coupling).

We select  $\beta = 5.9421$  for which there is a series of 100 000 lattices in a  $12^4$  box available. We complement this with  $L/a = 10, 14, 16, 18, 20, 22$ , thus spanning the range  $2.07 \leq L/r_0 \leq 4.54$ , as opposed to  $1.65 \leq L/r_0 \leq 3.86$  in Sec. 6. The details of these “post-production ensembles” are listed in Tab. 11. A technical point is that the statistical precision of  $Z_q$ , as listed in this table, degrades for large volumes. In line with Ref. [6] and our procedure in Sec. 6 we use, in the analysis below, the



$L/a$	$\beta$	$\langle q_{\text{ren}}^2 \rangle$	$\langle q_{\text{ren}}^4 \rangle / \langle q_{\text{ren}}^2 \rangle^2 - 3$	$\langle q_{\text{ren}}^4 \rangle / \langle q_{\text{ren}}^2 \rangle - 3\langle q_{\text{ren}}^2 \rangle$	$\langle q_{\text{ren}}^4 \rangle - 3\langle q_{\text{ren}}^2 \rangle^2$
10	5.9421	1.1095(38)	0.385(14)	0.427(15)	0.474(17)
12	5.9421	2.450(13)	0.135(20)	0.331(48)	0.81(12)
14	5.9421	4.546(10)	0.0550(74)	0.250(34)	1.14(15)
16	5.9421	7.664(20)	0.0225(85)	0.173(65)	1.32(50)
18	5.9421	12.257(31)	0.0408(84)	0.50(10)	6.1(1.3)
20	5.9421	18.557(36)	0.0221(61)	0.41(11)	7.6(2.1)
22	5.9421	27.251(49)	0.0237(57)	0.65(15)	17.5(4.2)

Table 12: *Ensemble average and statistical error of the squared topological charge and the three kurtosis definitions for the ensembles listed in Tab. 11. Throughout the “7stout” strategy is used.*

value  $Z_q = 1.2757(18)$  of the  $12^4$  box for all volumes.

On these ensembles we measure the topological susceptibility  $\langle q_{\text{ren}}^2 \rangle / V$  and the same excess kurtosis varieties as in Sec. 6. Again we limit ourselves to the “7stout” smoothing strategy. The results are listed in Tab. 12 and shown in Fig. 9. For comparison the old data ( $\beta = 6.1912$ ) are included. For the topological susceptibility some mild discretization effects are visible, but for the fourth-order cumulants they seem to be negligible at the current level of statistical precision.

We apply pure power-law fits  $c(L/r_0)^\alpha$  to the observables  $\langle q_{\text{ren}}^4 \rangle / \langle q_{\text{ren}}^2 \rangle^2 - 3$ ,  $\langle q_{\text{ren}}^4 \rangle / \langle q_{\text{ren}}^2 \rangle - 3\langle q_{\text{ren}}^2 \rangle$  and  $\langle q_{\text{ren}}^4 \rangle - 3\langle q_{\text{ren}}^2 \rangle^2$ . With the five largest volumes included, we find  $\alpha = -1.90(53)$ ,  $2.07(52)$  and  $5.98(52)$ , respectively, with  $P \simeq 0.23$  (in all three cases). And the prefactors  $c$  are  $0.40(26)$ ,  $0.027(17)$  and  $0.0019(12)$ , respectively, for these excess kurtosis varieties.

Note that the fitted power  $\alpha$  of the first excess kurtosis variety is negative by almost  $4\sigma$ . Hence, if  $\langle q_{\text{ren}}^4 \rangle / \langle q_{\text{ren}}^2 \rangle^2 - 3$  is used to quantify the deviation from a normal distribution, our fit says that any non Gaussian shape of the topological charge histogram is a finite-volume effect.

In addition, it is worth pointing out that the fitted powers  $\alpha$  are deceptively close to the integer values  $-2$ ,  $+2$  and  $+6$ , respectively. In view of the well known volume scaling law [8]

$$\langle q_{\text{ren}}^2 \rangle \propto L^4, \quad (23)$$

for the second cumulant, we conjecture the scaling laws

$$\langle q_{\text{ren}}^4 \rangle / \langle q_{\text{ren}}^2 \rangle^2 - 3 \propto L^{-2}, \quad \langle q_{\text{ren}}^4 \rangle / \langle q_{\text{ren}}^2 \rangle - 3\langle q_{\text{ren}}^2 \rangle \propto L^2, \quad \langle q_{\text{ren}}^4 \rangle - 3\langle q_{\text{ren}}^2 \rangle^2 \propto L^6 \quad (24)$$

for the three excess kurtosis varieties. Hence the first relation stipulates that  $\langle q_{\text{ren}}^4 \rangle / \langle q_{\text{ren}}^2 \rangle^2$  tends, in the infinite volume limit, to the value 3 in such a way that the difference is asymptotically suppressed by two powers of  $L$ . Similarly, the second relation says that  $\langle q_{\text{ren}}^4 \rangle / \langle q_{\text{ren}}^2 \rangle$  and  $3\langle q_{\text{ren}}^2 \rangle$  both grow like  $L^4$ , but the difference grows only like  $L^2$ . And the third relation suggests that  $\langle q_{\text{ren}}^4 \rangle$  and  $3\langle q_{\text{ren}}^2 \rangle^2$  individually grow like  $L^8$ , but the difference stays behind by two powers of  $L$ .

For the future we suggest studying, in the YM theory, the modified excess kurtosis varieties

$$\left[ \langle q_{\text{ren}}^4 \rangle / \langle q_{\text{ren}}^2 \rangle^2 - 3 \right] \frac{L^2}{r_0^2}, \quad \left[ \langle q_{\text{ren}}^4 \rangle / \langle q_{\text{ren}}^2 \rangle - 3\langle q_{\text{ren}}^2 \rangle \right] \frac{r_0^2}{L^2}, \quad \left[ \langle q_{\text{ren}}^4 \rangle - 3\langle q_{\text{ren}}^2 \rangle^2 \right] \frac{r_0^6}{L^6} \quad (25)$$

which we expect to assume universal (finite) values in the combined  $a \rightarrow 0, L \rightarrow \infty$  limit. Obviously, in these equations  $r_0$  [2] may be replaced by another suitable distance, e.g.  $t_0^{1/2}$  [3, 4] or  $w_0$  [5]. Our results for the respective constants  $c$  were mentioned in the text ahead of Eq. (23).

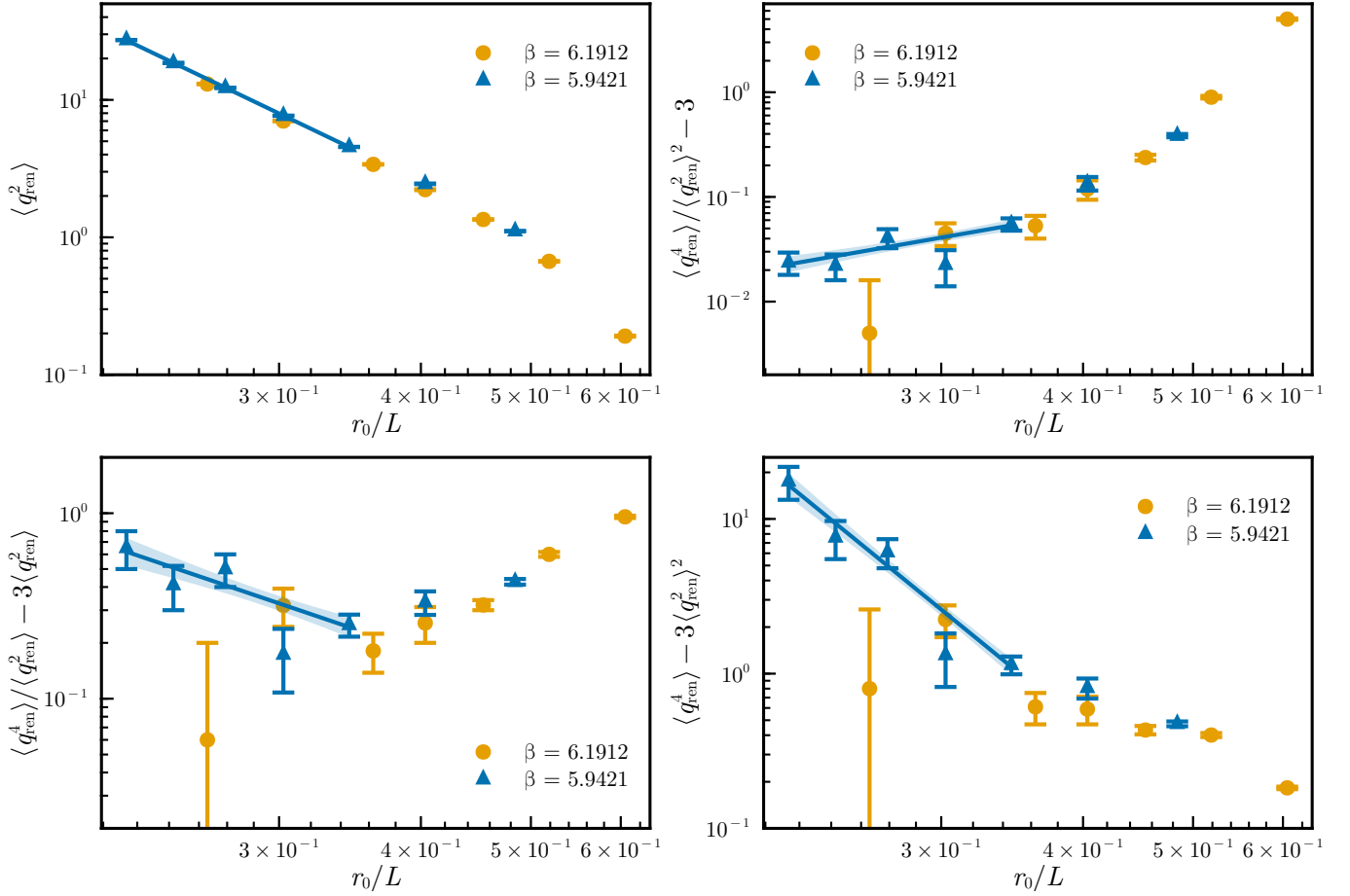


Figure 9: Large volume scaling of the topological susceptibility (top left) and of the three kurtosis varieties (remaining panels) with the “7stout” strategy. The new data ( $\beta = 5.9421$ , blue triangles) show mild cut-off effects relative to the old ones ( $\beta = 6.1912$ , orange circles), but they extend to larger box sizes. The power-law fits based on the five largest volumes suggest the scaling laws (24).

## References

- [1] S. Coleman, “Aspects of symmetry: Selected Erice lectures,” Cambridge University Press, 1985.
- [2] R. Sommer, “A new way to set the energy scale in lattice gauge theories and its applications to the static force and  $\alpha_s$  in SU(2) Yang-Mills theory,” Nucl. Phys. B **411**, 839-854 (1994) [arXiv:hep-lat/9310022].
- [3] M. Luscher, “Properties and uses of the Wilson flow in lattice QCD,” JHEP **08**, 071 (2010) [erratum: JHEP **03**, 092 (2014)] [arXiv:1006.4518 [hep-lat]].
- [4] M. Luscher and P. Weisz, “Perturbative analysis of the gradient flow in non-Abelian gauge theories,” JHEP **02**, 051 (2011) [arXiv:1101.0963 [hep-th]].
- [5] S. Borsanyi *et al.* [BMW], “High-precision scale setting in lattice QCD,” JHEP **09**, 010 (2012) [arXiv:1203.4469 [hep-lat]].
- [6] S. Durr, Z. Fodor, C. Hoelbling and T. Kurth, “Precision study of the SU(3) topological susceptibility in the continuum,” JHEP **04**, 055 (2007), [arXiv:hep-lat/0612021].
- [7] S. Necco and R. Sommer, “The N(f)=0 heavy quark potential from short to intermediate distances,” Nucl. Phys. B **622**, 328-346 (2002) [arXiv:hep-lat/0108008].

- [8] H. Leutwyler and A. V. Smilga, “Spectrum of Dirac operator and role of winding number in QCD,” *Phys. Rev. D* **46**, 5607-5632 (1992).
- [9] S. Durr, “Topological susceptibility in full QCD: Lattice results versus the prediction from the QCD partition function with granularity,” *Nucl. Phys. B* **611**, 281-310 (2001) [arXiv:hep-lat/0103011].
- [10] E. Witten, “Current algebra theorems for the U(1) Goldstone boson,” *Nucl. Phys. B* **156**, 269-283 (1979).
- [11] G. Veneziano, “U(1) without instantons,” *Nucl. Phys. B* **159**, 213-224 (1979).
- [12] Y. Aoki *et al.* [Flavour Lattice Averaging Group (FLAG)], “FLAG review 2021,” *Eur. Phys. J. C* **82**, no.10, 869 (2022) [arXiv:2111.09849 [hep-lat]].
- [13] E. Seiler and I. O. Stamatescu, “Some remarks on the Witten-Veneziano formula for the eta-prime mass,” MPI-PAE-PTh-10-87.
- [14] S. Chandrasekharan, “Lattice QCD with Ginsparg-Wilson fermions,” *Phys. Rev. D* **60**, 074503 (1999) [arXiv:hep-lat/9805015 [hep-lat]].
- [15] F. Niedermayer, “Exact chiral symmetry, topological charge and related topics,” *Nucl. Phys. B Proc. Suppl.* **73**, 105-119 (1999) [arXiv:hep-lat/9810026 [hep-lat]].
- [16] L. Giusti, G. C. Rossi and M. Testa, “Topological susceptibility in full QCD with Ginsparg-Wilson fermions,” *Phys. Lett. B* **587**, 157-166 (2004) [arXiv:hep-lat/0402027 [hep-lat]].
- [17] M. Campostrini, A. Di Giacomo, H. Panagopoulos and E. Vicari, “Topological charge, renormalization and cooling on the lattice,” *Nucl. Phys. B* **329**, 683-697 (1990).
- [18] A. Di Giacomo and E. Vicari, “Renormalization and topological susceptibility on the lattice,” *Phys. Lett. B* **275**, 429-434 (1992).
- [19] B. Alles, M. D’Elia, A. Di Giacomo and R. Kirchner, “A critical comparison of different definitions of topological charge on the lattice,” *Phys. Rev. D* **58**, 114506 (1998) [arXiv:hep-lat/9711026 [hep-lat]].
- [20] J. Hoek, M. Teper and J. Waterhouse, “Topological fluctuations and susceptibility in SU(3) lattice gauge theory,” *Nucl. Phys. B* **288**, 589-627 (1987).
- [21] B. Lucini and M. Teper, “SU(N) gauge theories in four-dimensions: Exploring the approach to N = infinity,” *JHEP* **06**, 050 (2001) [arXiv:hep-lat/0103027 [hep-lat]].
- [22] L. Del Debbio, H. Panagopoulos and E. Vicari, “theta dependence of SU(N) gauge theories,” *JHEP* **08**, 044 (2002) [arXiv:hep-th/0204125 [hep-th]].
- [23] C. Alexandrou, A. Athenodorou, K. Cichy, A. Dromard, E. Garcia-Ramos, K. Jansen, U. Wenger and F. Zimmermann, “Comparison of topological charge definitions in lattice QCD,” *Eur. Phys. J. C* **80**, no.5, 424 (2020) [arXiv:1708.00696 [hep-lat]].
- [24] C. Morningstar and M. J. Peardon, “Analytic smearing of SU(3) link variables in lattice QCD,” *Phys. Rev. D* **69**, 054501 (2004) [arXiv:hep-lat/0311018].
- [25] R. Narayanan and H. Neuberger, “Infinite N phase transitions in continuum Wilson loop operators,” *JHEP* **03**, 064 (2006) [arXiv:hep-th/0601210].
- [26] S. Capitani, S. Durr and C. Hoelbling, “Rationale for UV-filtered clover fermions,” *JHEP* **11**, 028 (2006) [arXiv:hep-lat/0607006 [hep-lat]].
- [27] M. Nagatsuka, K. Sakai and S. Sasaki, “Equivalence between the Wilson flow and stout-link smearing,” *Phys. Rev. D* **108**, no.9, 094506 (2023) [arXiv:2303.09938 [hep-lat]].
- [28] M. Ammer and S. Durr, “Stout smearing and Wilson flow in lattice perturbation theory,” *Phys. Rev. D* **110**, no.5, 5 (2024) [arXiv:2406.03493 [hep-lat]].

- [29] C. Bonanno, “The topological susceptibility slope  $\chi'$  of the pure-gauge SU(3) Yang-Mills theory,” JHEP **01**, 116 (2024) [arXiv:2311.06646 [hep-lat]].
- [30] M. Creutz, “Monte Carlo study of quantized SU(2) gauge theory,” Phys. Rev. D **21**, 2308-2315 (1980).
- [31] N. Cabibbo and E. Marinari, “A new method for updating SU(N) matrices in computer simulations of gauge theories,” Phys. Lett. B **119**, 387-390 (1982).
- [32] K. Fabricius and O. Haan, “Heat bath method for the twisted Eguchi-Kawai Model,” Phys. Lett. B **143**, 459-462 (1984).
- [33] A. D. Kennedy and B. J. Pendleton, “Improved heat bath method for Monte Carlo calculations in lattice gauge theories,” Phys. Lett. B **156**, 393-399 (1985).
- [34] S. L. Adler, “An overrelaxation method for the Monte Carlo evaluation of the partition function for multiquadratic actions,” Phys. Rev. D **23**, 2901 (1981).
- [35] M. Creutz, “Overrelaxation and Monte Carlo simulation,” Phys. Rev. D **36**, 515 (1987).
- [36] F. R. Brown and T. J. Woch, “Overrelaxed heat bath and Metropolis algorithms for accelerating pure gauge Monte Carlo calculations,” Phys. Rev. Lett. **58**, 2394 (1987).
- [37] D. B. Leinweber, A. G. Williams, J. B. Zhang and F. X. Lee, “Topological charge barrier in the Markov chain of QCD,” Phys. Lett. B **585**, 187-191 (2004) [arXiv:hep-lat/0312035 [hep-lat]].
- [38] S. Durr, “Gauge action improvement and smearing,” Comput. Phys. Commun. **172**, 163-186 (2005) [arXiv:hep-lat/0409141 [hep-lat]].
- [39] C. Bonati, M. D’Elia and A. Scapellato, “ $\theta$  dependence in SU(3) Yang-Mills theory from analytic continuation,” Phys. Rev. D **93**, no.2, 025028 (2016) [arXiv:1512.01544 [hep-lat]].
- [40] C. Alexandrou *et al.* [ETM Collaboration], “Probing the energy-smear R ratio using lattice QCD,” Phys. Rev. Lett. **130**, no.24, 241901 (2023) [arXiv:2212.08467 [hep-lat]].
- [41] C. Bonanno, F. D’Angelo and M. D’Elia, “The chiral condensate of  $N_f=2+1$  QCD from the spectrum of the staggered Dirac operator,” JHEP **11**, 013 (2023) [arXiv:2308.01303 [hep-lat]].
- [42] T. M. B. Asmussen, R. Hollwieser, F. Knechtli and T. Korzec, “The determination of potential scales in 2+1 flavor QCD,” [arXiv:2412.10215 [hep-lat]].
- [43] M. Luscher, “Volume dependence of the energy spectrum in massive quantum field theories. 1. Stable particle states,” Commun. Math. Phys. **104**, 177 (1986)
- [44] A. Athenodorou and M. Teper, “SU(N) gauge theories in 3+1 dimensions: Glueball spectrum, string tensions and topology,” JHEP **12**, 082 (2021) [arXiv:2106.00364 [hep-lat]].
- [45] M. Luscher and F. Palombi, “Universality of the topological susceptibility in the SU(3) gauge theory,” JHEP **09**, 110 (2010) [arXiv:1008.0732 [hep-lat]].
- [46] L. Del Debbio, L. Giusti and C. Pica, “Topological susceptibility in the SU(3) gauge theory,” Phys. Rev. Lett. **94**, 032003 (2005) [arXiv:hep-th/0407052 [hep-th]].
- [47] L. Giusti, M. Luscher, P. Weisz and H. Wittig, “Lattice QCD in the epsilon regime and random matrix theory,” JHEP **11**, 023 (2003) [arXiv:hep-lat/0309189 [hep-lat]].
- [48] S. O. Bilson-Thompson, D. B. Leinweber and A. G. Williams, “Highly improved lattice field strength tensor,” Annals Phys. **304**, 1-21 (2003) [arXiv:hep-lat/0203008 [hep-lat]].